Steady-state model for the electron beam pumped KrF laser

W.J. WITTEMAN

Department of Applied Physics, Twente University of Technology, Enschede, The Netherlands

Abstract. In this paper the kinetics of excitation, quenching, and absorption in an e-beam pumped KrF laser is discussed. It is argued that under usual experimental conditions the steady-state approximation can be applied. For that case a comprehensive kinetic model can be treated analytically. The model simulates quite well the experimental results obtained so far. It predicts the maximum performance conditions, limiting behaviour, and scaling properties of e-beam pumped KrF lasers.

1. Introduction

Rare-gas fluoride exciplexes (KrF*, XeF*, and ArF*) are used as active media to obtain the most powerful and efficient UV lasers to date. An output energy of 24 Joule/liter has been obtained with KrF* at an efficiency of about 8 percent [10]. The exciplexes can be produced in a gas mixture containing the rare gas, fluorine and a buffer gas. The excitation is achieved by irradiation with a relativistic electron beam, an electron beam controlled discharge or an UV preionized discharge. The best results are obtained by pure electron-beam excitation. The usual gas mixture for an electron-beam pumped KrF laser is 2–6 Torr F_2, 100–200 Torr Kr and 2–4 atm. Ar. The lasing species, KrF*, is mainly formed from ions in the reaction

$$Kr^+ + F^- \rightarrow KrF^*.$$

The krypton ions are either produced directly by the interaction of the electron beam with Kr or at the end of a reaction chain starting from ionized argon. The secondary electrons from the ionization process undergo easily dissociative attachment with F_2 to form F^- ions.

Although there is in principle also a 'neutral channel', starting with metastable atoms to form KrF*, this channel is not important, because only a fraction (15–20%) of the electron energy is used to produce metastable states. Moreover, the sequence reactions in the neutral channel are relatively slower than those with ions, so that an even smaller part of the electron energy goes through the neutral channel. Numerical calculations show that for an electron beam pumped system the formation kinetics in the case of short pulses (25–50 ns) goes for more than 90% through the ion channel. Therefore we consider only the ion channel. The kinetic of the KrF* is characterized by a chain of many chemical reactions. The most important reactions and rate constants have been extensively studied in the past and are described in literature [6, 7, 13]. In the following we shall use the knowledge of these reactions to describe a model that includes the most important kinetic processes in the laser mechanism. It will be argued that under the

Applied Scientific Research 37: 195–208 (1981) 0003–6994/81/0372–0195 $02.10

Table 1. Dominant formation rate constants

Reaction	Reaction constant	Reference
$Ar^+ + 2Ar \rightarrow Ar_2^+ + Ar$	$k_1 = 2.5 \times 10^{-31}$ cm^6 S^{-1}	[2]
$Ar_2^+ + Kr \rightarrow Kr^+ + 2Ar$	$k_2 = 7.5 \times 10^{-10}$ cm^3 S^{-1}	[8]
$Kr^+ + F^- \rightarrow KrF^*$	$k_3 = 3 \times 10^{-6}$ cm^3 S^{-1}	[5]
$Ar^+ + F^- \rightarrow ArF^*$	$k_3' = 3 \times 10^{-6}$ cm^3 S^{-1}	[5]
$Ar_2^+ + F^- \rightarrow ArF^* + Ar$	$k_3'' = 3 \times 10^{-6}$ cm^3 S^{-1}	[5]
$Kr^+ + Kr + Ar \rightarrow Kr_2^+ + Ar$	$k_{10} = 2.5 \times 10^{-31}$ cm^6 S^{-1}	[9]
$Kr_2^+ + F^- \rightarrow KrF^* + Kr$	$k_3''' = 3 \times 10^{-6}$ cm^3 S^{-1}	[5]
$ArF^* + 2Ar \rightarrow Ar_2F^* + Ar$	$k_{13} = 5 \times 10^{-32}$ cm^6 S^{-1}	[7]
$ArF^* + Kr \rightarrow KrF^* + Ar$	$k_{11} = 3 \times 10^{-10}$ cm^3 S^{-1}	[9]
$ArF^* + F_2 \rightarrow Ar + F + F_2$	$k_8 = 1.9 \times 10^{-9}$ cm^3 S^{-1}	[12]
$KrF^* + Ar \rightarrow Kr + Ar + F$	$k_4 = 1.8 \times 10^{-12}$ cm^3 S^{-1}	[4]
$KrF^* + 2Ar \rightarrow ArKrF^* + Ar$	$k_5 = 8 \times 10^{-32}$ cm^6 S^{-1}	[9]
$KrF^* + Ar + Kr \rightarrow Kr_2F^* + Ar$	$k_6 = 6.5 \times 10^{-31}$ cm^6 S^{-1}	[9]
$KrF^* + F_2 \rightarrow Kr + F + F_2$	$k_7 = 5.2 \times 10^{-10}$ cm^3 S^{-1}	[4]
$KrF^* + e \rightarrow$ products	$\alpha = 2 \times 10^{-7}$ cm^3 S^{-1}	[15]
$ArF^* + e \rightarrow$ products	$\alpha = 2 \times 10^{-7}$ cm^3 S^{-1}	[15]
$Ar_2F^* + Kr \rightarrow ArKrF^* + Ar$	$k_{14} = 1 \times 10^{-10}$ cm^3 S^{-1}	[7]
$Ar_2F^* + F_2 \rightarrow 2Ar + F + F_2$	$k_9 = 1 \times 10^{-9}$ cm^3 S^{-1}	[7]
$ArKrF^* + Kr \rightarrow Kr_2F^* + Ar$	$k_{17} = 2 \times 10^{-11}$ cm^3 S^{-1}	[9]
$ArKrF^* + Kr \rightarrow Ar_2F^* + Kr$	$k_{18} = 2 \times 10^{-11}$ cm^3 S^{-1}	[9]
$Kr_2F^* + 2A \rightarrow 2Kr + F + 2A$	$k_{19} = 1 \times 10^{-31}$ cm^6 S^{-1}	[1]
$Kr_2F^* + F_2 \rightarrow 2Kr + F + F_2$	$k_{20} = 1 \times 10^{-9}$ cm^3 S^{-1}	[7]
$F_2 + e \rightarrow F^- + F$	$\beta = 2 \times 10^{-9}$ cm^3 S^{-1}	[9]

usual experimental conditions a steady-state model can be derived. With such a model an analytic solution of the rate equations is obtained. The dependence of the radiation production on the basic processes in the kinetic chain is obtained and the conditions for optimum performance of the laser system can be predicted. Finally, we shall discuss the relation between the model and experimental results obtained so far with high-power systems.

2. Kinetics

The kinetics of the KrF laser is initiated by the electron-beam interaction with a gas mixture of Ar, Kr, and F_2. The interaction is complicated and many new species are formed. The most important reactions and rate coefficients are listed in Tables 1 and 2. A flow diagram of the kinetics is shown in Figure 1.

The transfer of electron energy to the argon gas is proportional to the density [Ar], so that the ion-production rate can be written as P[Ar], where P, depending on current density and energy, is the average ionization rate of an argon atom. There is also some production of Ar^+ by the intracavity radiation absorption process of Ar_2^+. On the other hand, ions are lost by collision with argon to form Ar_2^+ and by collision with F^- to form ArF*. We obtain the following rate equation:

Table 2. Dominant radiation interaction

Reaction	Cross-section/Time constant	Reference
$KrF^* + h\nu \rightarrow Kr + F + 2h\nu$	$\sigma_s = 2.4 \times 10^{-16}$ cm^2	[7], [14]
$Ar_2^+ + h\nu \rightarrow Ar^+ + Ar$	$\sigma_1 = 1.5 \times 10^{-17}$ cm^2	[8]
$Kr_2^+ + h\nu \rightarrow Kr^+ + Kr$	$\sigma_2 = 1.5 \times 10^{-17}$ cm^2	[7], [14]
$Kr_2F^* + h\nu \rightarrow$ products	$\sigma_3 = 5 \times 10^{-18}$ cm^2	[7]
$F_2 + h\nu \rightarrow 2F$	$\sigma_4 = 1.5 \times 10^{-20}$ cm^2	[8]
$F^- + h\nu \rightarrow F + e$	$\sigma_5 = 5.6 \times 10^{-18}$ cm^2	[8]
$KrF^* \rightarrow Kr + F + h\nu$	$\tau_1 = 6 \times 10^{-9}$ sec	[7], [14]
$ArF^* \rightarrow Ar + F + h\nu$	$\tau_2 = 4 \times 10^{-9}$ sec	[3]
$Ar_2F^* \rightarrow 2Ar + F + h\nu$	$\tau_3 = 5 \times 10^{-9}$ sec	[7]
$ArKrF^* \rightarrow Ar + Kr + F + h\nu$	$\tau_4 = 2 \times 10^{-8}$ sec	[7]
$Kr_2F^* \rightarrow 2Kr + F + h\nu$	$\tau_5 = 1.5 \times 10^{-8}$ sec	[7]

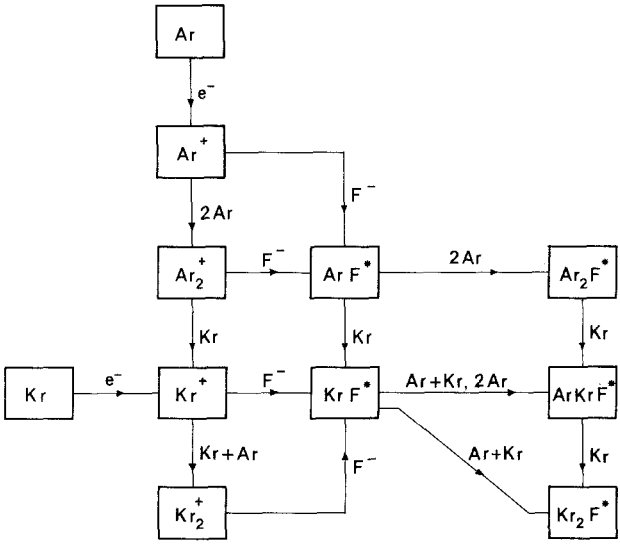

Figure 1. Flow diagram representing the most important kinetics of an e-beam pumped KrF laser

$$\frac{d[Ar^+]}{dt} = P[Ar] + \sigma_1 [Ar_2^+] I - k_1 [Ar^+] [Ar]^2 - k_3' [Ar^+] [F^-], \tag{1}$$

where k_1 is the formation constant of molecular argon ions, σ_1 the absorption cross-section, and k_3' the formation constant for ArF*.

The main processes suffered by the molecular argon ions are the ionization of krypton, with a rate constant k_2, the formation of ArF*, with a rate constant k_3'', and the photoabsorption by the intracavity radiation field (cross-section σ_1):

$$\frac{d[Ar_2]}{dt} = k_1 [Ar^+] [Ar]^2 - \sigma_1 [Ar_2^+] I - k_2 [Kr] [Ar_2^+] - k_3'' [Ar_2^+] [F^-]. \tag{2}$$

The rate equation for Kr^+ contains the direct production by the electron beam and the formation by Ar_2^+. The ions form KrF* by the Coulomb interaction with F^-. Further some ions produce Kr_2^+ in collisions with Ar and Kr. The rate constants are respectively k_3 and k_{10}:

$$\frac{d[Kr^+]}{dt} = 2P[Kr] + k_2[Ar_2^+][Kr] - k_3[Kr^+][F^-] - k_{10}[Kr^+][Kr][Ar]. \quad (3)$$

The ionization rate per Kr atom is about twice that for Ar, hence the factor 2 in the first term.

The formed Kr_2^+ species have also Coulomb interaction with F^- to create KrF* with rate constant k_3'''. There is also absorption by the radiation (cross-section σ_2):

$$\frac{d[Kr_2^+]}{dt} = k_{10}[Kr^+][Kr][Ar] - k_3'''[Kr_2^+][F^-] - \sigma_2[Kr_2^+]I. \quad (4)$$

The ArF* species form KrF* in a replacement reaction with Kr with a rate constant k_{11}. Further, ArF* is lost by three body collisions with Ar to produce Ar_2F^* with a rate constant k_{13}, by quenching in collisions with F_2 (rate constant k_8) and electrons (density $[n]$ and rate constant α), and through radiative decay (time constant τ_2):

$$\frac{d[ArF^*]}{dt} = k_3'[Ar^+][F^-] + k_3''[Ar_2^+][F^-] - k_{11}[ArF^*][Kr] - \alpha[ArF^*][n] + - k_{13}[ArF^*][Ar]^2 - k_8[ArF^*][F_2] - \frac{1}{\tau_2}[ArF^*]. \quad (5)$$

The lasing species KrF* formed in the above mentioned processes are balanced by the process of stimulated emission, with cross-section σ_s, quenching by electrons, two and three body collisions with Ar, Kr, and F_2, and by radiative decay with time constant τ_1:

$$\frac{d[KrF^*]}{dt} = k_3[Kr^+][F^-] + k_3'''[Kr_2^+][F^-] + k_{11}[ArF^*][Kr] + - (\sigma_s I + Q_1)[KrF^*], \quad (6)$$

where

$$Q_1 = \alpha[n] + k_4[Ar] + k_5[Ar]^2 + k_6[Kr][Ar] + k_7[F_2] + \frac{1}{\tau_1} \quad (7)$$

is the parameter describing quenching and radiative decay.

The Ar_2F^* species are quenched by Kr, Ar, and F_2 and have a radiative decay time of τ_3 sec:

$$\frac{d[\mathrm{Ar_2F^*}]}{dt} = k_{13}[\mathrm{ArF^*}][\mathrm{Ar}]^2 + k_{18}[\mathrm{ArKrF^*}][\mathrm{Ar}] + - \left(k_{14}[\mathrm{Kr}] + k_9[\mathrm{F_2}] + \frac{1}{\tau_3}\right)[\mathrm{Ar_2F^*}]. \quad (8)$$

The ArKrF* species formed in collisions of Ar_2F^* and KrF* with Kr and Ar are also quenched in collisions with Kr and Ar to produce Kr_2F^* (rate constant k_{17}) and Ar_2F^* (rate constant k_{18}). Further there is radiative decay with a time constant τ_4:

$$\frac{d}{dt}[\mathrm{ArKrF^*}] = k_{14}[\mathrm{Ar_2F^*}][\mathrm{Kr}] + k_5[\mathrm{KrF^*}][\mathrm{Ar}]^2 + - k_{17}[\mathrm{ArKrF^*}][\mathrm{Kr}] - k_{18}[\mathrm{ArKrF^*}][\mathrm{Ar}] + - \frac{1}{\tau_4}[\mathrm{ArKrF^*}]; \quad (9)$$

$$\frac{d}{dt}[\mathrm{Kr_2F^*}] = k_6[\mathrm{KrF^*}][\mathrm{Ar}][\mathrm{Kr}] + k_{17}[\mathrm{ArKrF^*}][\mathrm{Kr}] + - k_{19}[\mathrm{Kr_2F^*}][\mathrm{Ar}]^2 - k_{20}[\mathrm{Kr_2F^*}][\mathrm{F_2}] + - \frac{1}{\tau_5}[\mathrm{Kr_2F}] - \sigma_3[\mathrm{Kr_2F^*}]I. \quad (10)$$

In the discharge medium we assume neutrality. The dominant loss of secondary electrons is rapid dissociative attachment with F_2 with rate constant β, resulting in F^- formation. So we can write for the electron density:

$$\frac{d[n]}{dt} = P[\mathrm{A} + 2\mathrm{K}] - \beta[n][\mathrm{F_2}], \quad (11)$$

where the electron density is given by

$$[n] = [\mathrm{Ar^+}] + [\mathrm{Ar_2^+}] + [\mathrm{Kr^+}] + [\mathrm{Kr_2^+}] - [\mathrm{F^-}]. \quad (12)$$

The radiation field within the cavity is mainly subjected to stimulated emission, outcoupling, and absorption by Ar_2^+, Kr_2^+, F^-, Kr_2F^* and F_2. We obtain the following equation for the photon density flux:

$$\frac{1}{c}\frac{dI}{dt} = \sigma_s I[\mathrm{KrF^*}] - \gamma I - \sigma_1 I[\mathrm{Ar_2^+}] - \sigma_2 I[\mathrm{Kr_2^+}] - \sigma_3 I[\mathrm{Kr_2F^*}], \quad (13)$$

where

$$\gamma = \gamma_0 + \gamma_a.$$

$\gamma_0 = (-\ln R)/2L$ is the well-known outcoupling factor for a cavity having a value R for the product of the reflectivities of the mirrors separated at a distance L,

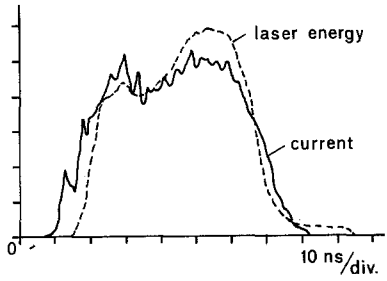

Figure 2. The time behaviour of a current pulse of about 50 nsec (solid line) and the corresponding laser output pulse (broken line)

$$\gamma_a = \sigma_{F^-}[F^-] + \sigma_{F_2}[F_2] \tag{14}$$

being the absorption loss by the fluorine ions and molecules.

The absorption of F^- and F_2 turns out to be very small compared to those of Ar_2^+ and Kr_2^+. Moreover, the calculations show that F^- is practically independent of the excitation parameter P. For these reasons we take the losses due to F^- and F_2 and the outcoupling together.

For the laser parameters used in the range of maximum operation performance it is found that the time constants for the species and the output power following the excitation pulse is in the order of a few nanoseconds. This is found by a numerical evaluation of the above equations, but also from experiments. In fact, we observed that the radiation pulse follows rather accurately the shape of the excitation pulse (Figure 2). This means that for an excitation process during a time larger than those time constants the laser process can be considered quasi-stationary. The stationary process yields the great advantage of an analytic treatment of the complicated kinetics of this laser process. This allows us to determine directly the effects of the partial pressure of gas components, excitation density and cavity on the various formation, quenching and absorption processes. In this way optimum performance conditions are easily obtained.

3. Quasi-stationary solution of the rate equations

Adding equation (1) to (6) we obtain for the stationary state:

$$P\{2[Kr] + [Ar]\} - [ArF^*]\left\{k_{13}[Ar]^2 + k_8[F_2] + \frac{1}{\tau_2} + \alpha[n]\right\} +$$

$$-I\sigma_2[Kr_2^+] = (I\sigma_s + Q_1)[KrF^*]. \tag{15}$$

From the radiation equation for the cavity (12) we obtain:

$$[KrF^*] = \frac{1}{\sigma_s}\left\{\gamma + \sigma_1[Ar_2^+] + \sigma_2[Kr_2^+] + \sigma_3[Kr_2F^*]\right\}. \tag{16}$$

Substituting (16) into (15) we finally obtain:

$$W/P = \frac{\bar{\gamma}\{[\mathrm{Ar}] + 2[\mathrm{Kr}] - Q_2[\mathrm{ArF}^*]P^{-1} - Q_1\sigma_s^{-1}(\bar{\gamma} + \sigma_1[\mathrm{Ar}_2^+]P^{-1} + \sigma_2[\mathrm{Kr}_2^+]P^{-1} + \sigma_3[\mathrm{Kr}_2\mathrm{F}^*]P^{-1})\}}{\bar{\gamma} + \sigma_1[\mathrm{Ar}_2^+]P^{-1} + 2\sigma_2[\mathrm{Kr}_2^+]P^{-1} + \sigma_3[\mathrm{KrF}^*]P^{-1}} \tag{17}$$

where $W = \gamma I$ is the production rate of photons per unit volume, $\bar{\gamma} = \gamma/P$, and

$$Q_2 = k_{13}[\mathrm{Ar}]^2 + k_8[\mathrm{F}_2] + \alpha[n] + \frac{1}{\tau_2} \tag{18}$$

is the quenching parameter of ArF*.

From equation (17) we can calculate W/P as a function of P/γ with the gas densities as parameters. Then we find W/P to depend strongly on the densities of Ar and Kr but little on F_2, if we substitute for F_2 the usual experimental pressures of a few Torr. Therefore we have kept F_2 constant and equal to 10^{17} cm^{-3}.

We also calculated the maximum produced photons per excitation or the maximum values of W/P as a function of P/γ together with the corresponding densities of Ar and Kr. In Figure 3 the maximum values of W/P are plotted versus P/γ with P as parameter. It is seen that the output has a maximum for P/γ, but its dependence on P/γ is only significant for low pumping rates or high outcoupling. The corresponding densities of Ar and Kr for which the maxima are obtained are plotted in Figures 4 and 5 respectively.

The most important species Ar^+, Ar_2^+, Kr^+, Kr_2^+, F^- and n (electron density) formed in the laser mixture under the maximum output conditions are plotted in Figures 6, 7, 8, 9, 10 and 11 respectively, again versus P/γ with P as parameter. The corresponding Ar and Kr densities are those indicated in Figures 4 and 5 respectively.

We define the efficiency of the laser process as

$$\eta = \frac{W}{P}([\mathrm{Ar}] + 2[\mathrm{Kr}]) \tag{19}$$

being the ratio of the photon density rate and the excitation rate density. In other words the efficiency describes the change that an atom ionized by the fast electrons leads to the production of a photon that is coupled out. This is not exactly true because W includes both the outcoupled photons and those absorbed by the species F^- and F_2. However the latter two absorptions are in the range of interest about two orders of magnitude smaller than the outcoupling. The values of η for optimum output versus P/γ are plotted in Figure 12 with P as parameter. The efficiency describing the relation between radiation output and electrical input energy is smaller because the energy loss per argon ionization is estimated as about 26 eV, whereas the outcoming photon has an energy of 5 eV. Thus with a quantum efficiency of about 0.2 we predict an overall efficiency for the electron energy between 8 and 10 percent.

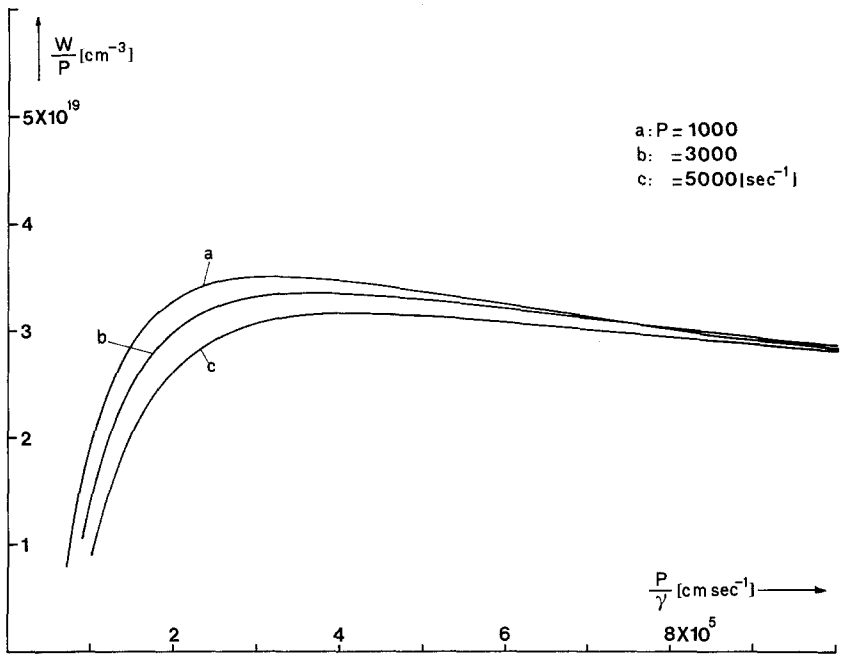

Figure 3. The ratio of maximum extracted photon density to the average excitation rate versus the ratio of the excitation rate to the outcoupling. The parameter is the excitation rate per atom

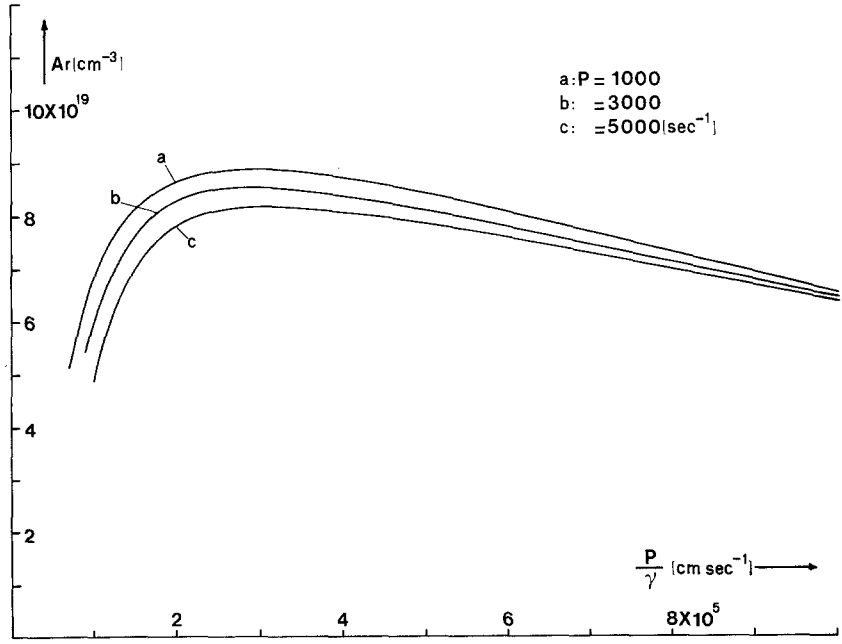

Figure 4. The argon densities for which the maximum output is obtained versus the ratio of the excitation rate to the coupling

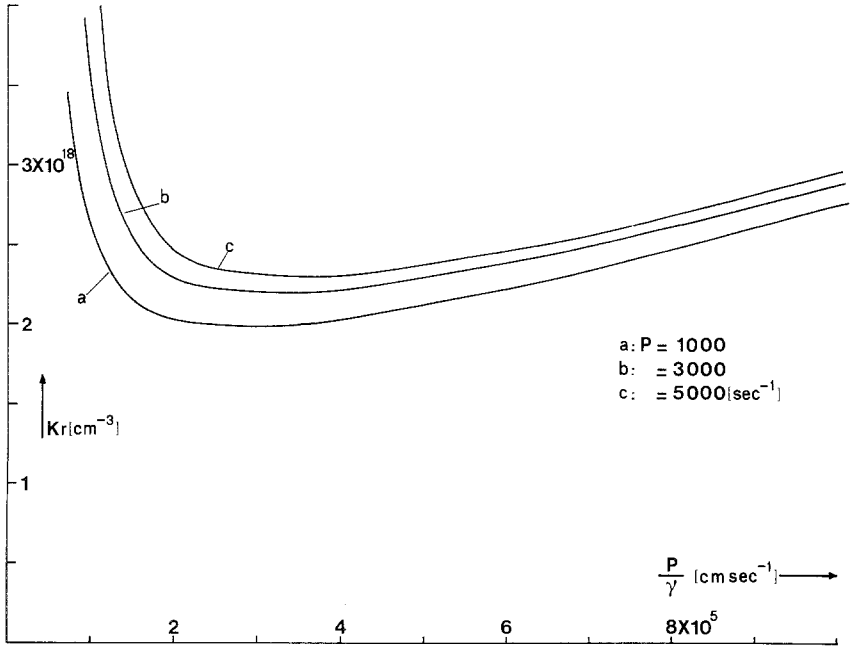

Figure 5. The krypton densities for which the maximum output is obtained versus the ratio of the excitation rate to the outcoupling

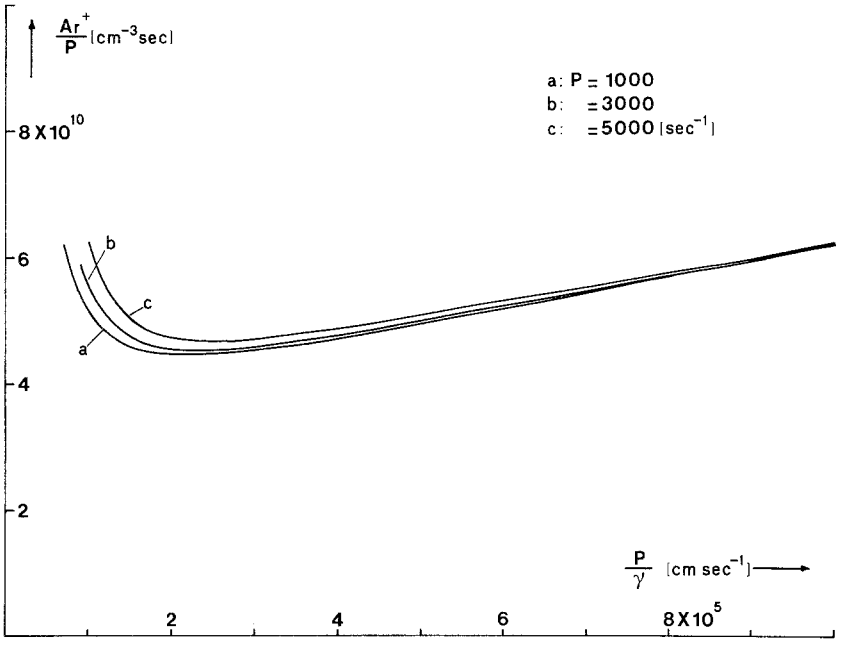

Figure 6. The argon ion density divided by P for optimum output conditions as a function of P/γ

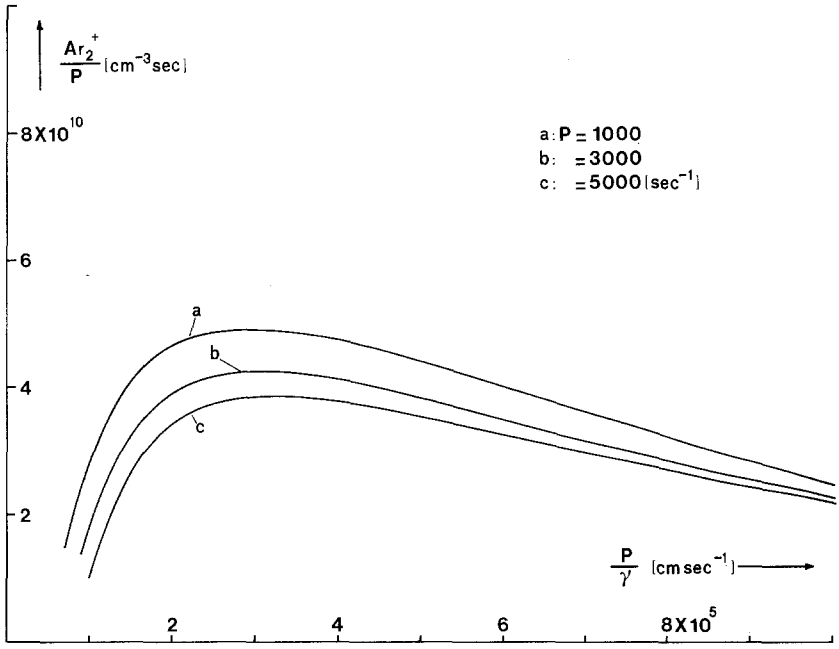

Figure 7. The molecular argon density divided by P for optimum output conditions versus P/γ

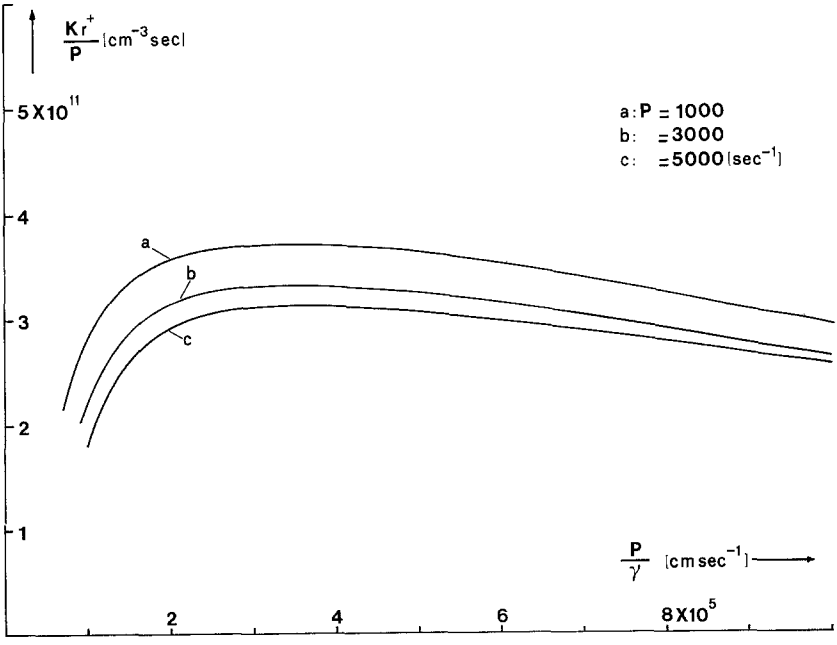

Figure 8. The krypton ion density divided by P for optimum output conditions versus P/γ

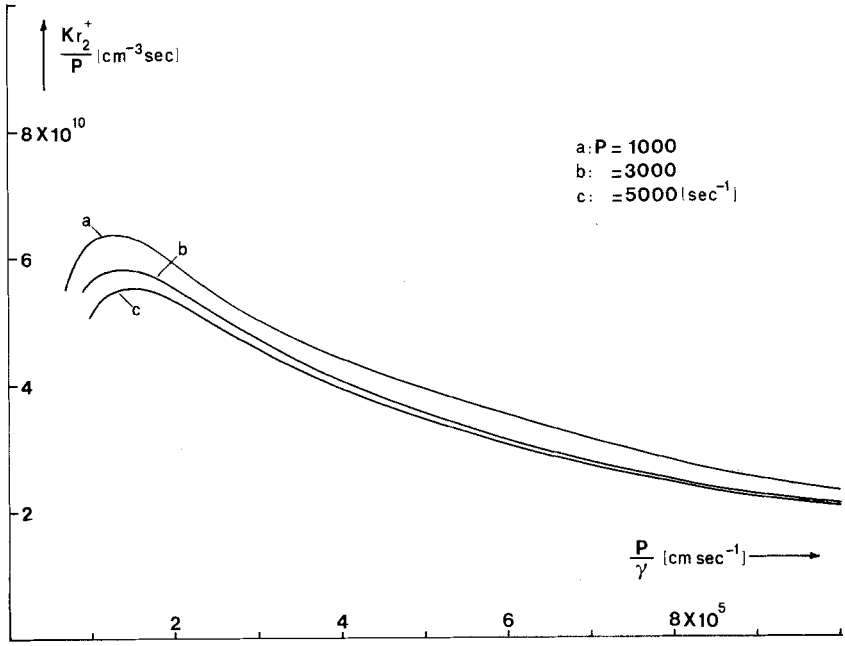

Figure 9. The molecular krypton density divided by P for optimum output conditions versus P/γ

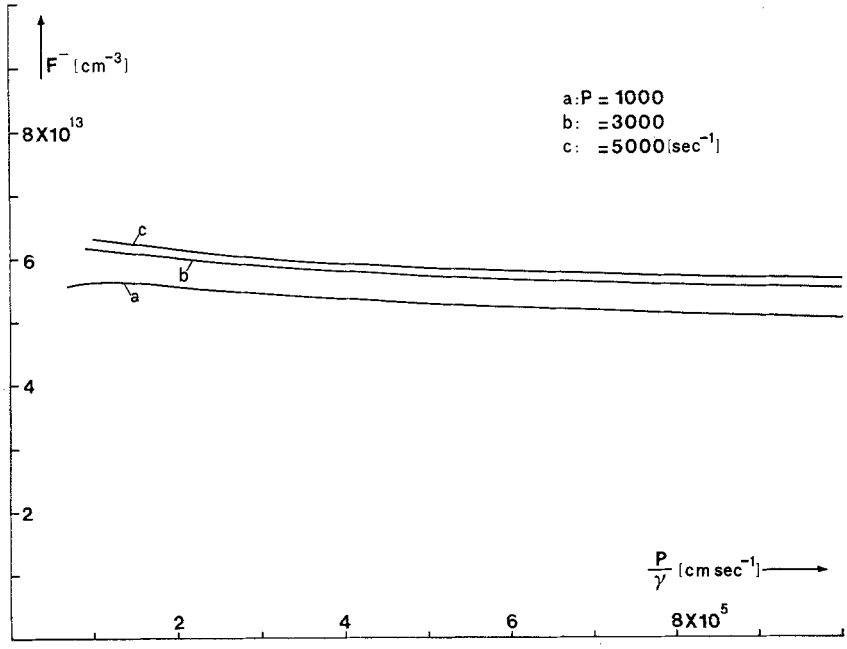

Figure 10. The density of F^- for optimum output conditions versus P/γ. It is found that F^- is practically constant and independent on P

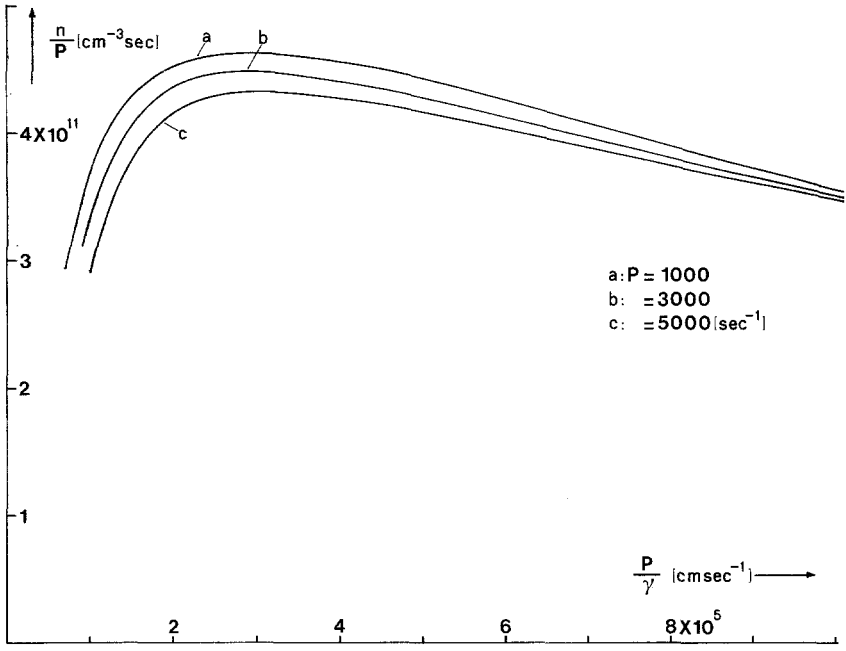

Figure 11. The electron density divided by P for optimum output conditions versus P/γ

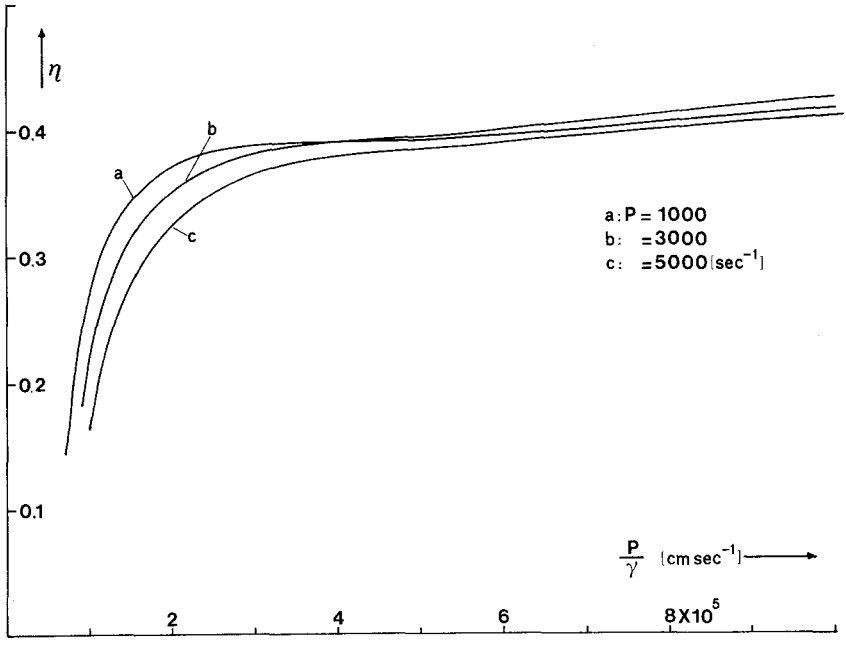

Figure 12. The efficiency η that corresponds with the maximum output power versus P/γ

4. Discussion of the model

The predictions described in the previous section are in good agreement with our experiments, which are reported in ref. [10, 11, 16]. It is observed that the maximum output energy is not very sensitive to the Kr density. The observed maximum density is about 3×10^{18} cm^{-3} and in substantial agreement with the model. It should be noted that Kr has a broad maximum. Similarly we observed that at maximum operation conditions the argon density is around 9×10^{19} cm^{-3} (3.6 atm). This is in good agreement with our model. Further increase of the excitation current density does not require higher argon densities as expected. Also the outcoupled photon density and overall efficiency between 8 and 10 percent are in excellent agreement with our observations.

For the optimum performance conditions with respect to output we found from the model that most excimer energy of KrF* is lost by quenching. The losses by radiation absorption are minor. For low values of P/γ, say smaller than 2×10^5 cm/sec, the system is inefficient due to quenching by Ar and Kr. At higher values the system has a broad maximum for P/γ. This was also observed experimentally by increasing the reflectivity of the outcoupling mirror from 8 to 16 percent for a system with high excitation density. The decrease of W/P at the right of the maxima in Figure 3 is due to increasing photon absorption by Ar_2^+ and Kr_2^+.

It is seen that the maximum values of W/P are primarily dependent on P/γ. The relatively small decrease of the values of W/P with increasing value of the excitation parameter P is due to electron quenching.

In order to compare the calculated W/P values with those obtained experimentally for a 50 nsec pulse at about 3.75 atm total gas pressure we multiply W/P by the corresponding P/γ value. We then find for our curves that W/P at maximum Ar gas pressure is about 10^{25}, which corresponds to $8 \cdot 10^6$ Watt per cm^2. Using the experimental outcoupling factor of about $3 \cdot 10^{-2}$, a volume of 600 cm^3 and a pulse duration of 50 nsec, we calculate 7.5 Joule output energy. The experimental output energy is 10.2 Joule.

References

1. Basov NG, Danilychev VA, Dolgikh VA, Kerimov OM, Lebedev VS and Molchanov AG (1979) Kinetics of excimer formation in lasers utilizing rare-gas fluorine mixtures. Sov J Quantum Electron 9: 593–597
2. McDaniel EW, Ermak V, Delgarno A, Ferguson EE and Friedman L (1970) Ion molecule reaction, Wiley-Interscience, New York
3. Dunning TH and Hay PJ (1978) The covalent and ionic states of the rare gas monofluorides. J Chem Phys 69: 134–149
4. Eden JG, Waynant WR, Searles SK and Burnham R (1978) New quenching rates applicable to the KrF laser. Appl Phys Lett 32: 733–735
5. Flannery MR and Yang TP (1978) Ionic recombination of rare gas atomic ions X^+ with F^- in a dense gas X. Appl Phys Lett 32: 327–329 and 32: 356–357

6. Hutchinson MHR (1980) Excimers and excimer lasers. Appl Phys 21: 95–114
7. Johnson TH and Hunter AM (1980) Physics of the krypton fluoride laser. J Appl Phys 51: 2406–2420
8. Lacina WB, Cohn DB (1978) Theoretical analysis of the electrically excited KrF laser. Appl Phys Lett 32: 106–108
9. Mangano JA, Jacob JH, Rokni M and Hanryluk A (1977) Three-body quenching of KrF* by Ar and broad-band emission at 415 mm. Appl Phys Lett 31: 26–28
10. Oomen GL (1981) Development and optimization of electron beam excited krypton-fluoride lasers. Thesis Twente University of Technology, Febr 1981.
11. Oomen GL and Witteman WJ (1980) A coaxial e-beam excitation system for high power excimer lasers. Optics Comm 32: 461–466
12. Rokni M, Jacob JH, Mangano JA and Brochu R (1977) Formation and quenching kinetics of ArF*. Appl Phys Lett 31: 79–81
13. Rokni M, Mangano JA, Jacob JH and Hsia JC (1978) Rare gas fluoride lasers. IEEE J Quantum Electron 14: 464–481
14. Tellinghuisen J, Hays AK, Hoffman JM and Tisone GC (1975) Spectroscopic studies of diatomic noble gas halides, J Chem Phys 65: 4473–4482
15. Trainor DW and Jacob JH (1980) Electron quenching of KrF* and ArF*. Appl Phys Lett 37: 675–677
16. Witteman WJ and Oomen GL (1980) On the performance of an e-beam pumped KrF laser. Optics Comm 32: 467–472